JGR Space Physics

Key Points:

- Scattering rates of electrons are quantified with the latest Jovian whistler-mode wave model from Juno PJ01-45 data
- Whistler-mode waves are able to accelerate MeV electrons in the middle magnetosphere of Jupiter in tens of days
- Electrons accelerated in the outer whistler-mode belt are further transported inward, indicating a two-step acceleration mechanism

Acceleration of Energetic Electrons in Jovian Middle Magnetosphere by Whistler-Mode Waves

Y.-X. Hao[1,2] (ID), Y. Y. Shprits[1,3,4] (ID), J. D. Menietti[5], T. Averkamp[5] (ID), D. D. Wang[1] (ID), P. Kollmann[6] (ID), G. B. Hospodarsky[5] (ID), A. Drozdov[4] (ID), A. Saikin[4], E. Roussos[2] (ID), N. Krupp[2] (ID), R. B. Horne[7] (ID), E. E. Woodfield[7] (ID), and S. J. Bolton[8] (ID)

[1]GFZ German Research Centre for Geosciences, Potsdam, Germany, [2]Max Planck Institute for Solar System Research, Goettingen, Germany, [3]Institute of Physics and Astrophysics, University of Potsdam, Potsdam, Germany, [4]University of California Los Angeles, Los Angeles, CA, USA, [5]Department of Physics and Astronomy, University of Iowa, Iowa City, IA, USA, [6]Johns Hopkins University Applied Physics Laboratory, Laurel, MD, USA, [7]British Antarctic Survey, Cambridge, UK, [8]Space Science and Engineering Division, Southwest Research Institute, San Antonio, TX, USA

Abstract An abundant multi-MeV electron population beyond the orbit of Io is required to explain the intense inner radiation belt (electrons > 50 MeV) at Jupiter and its synchrotron radiation. In order to better understand the synergistic effect of radial transport and local wave-particle interactions driven by whistler-mode waves on the formation of Jupiter's radiation belt, we perform 3-D Fokker-Planck simulations for Jovian energetic electrons with the Versatile Electron Radiation Belt code. An empirical model of Jovian whistler-mode waves updated with measurements from the Juno extended mission is used to quantify the local acceleration and pitch angle scattering. Resonant cyclotron acceleration by whistler-mode waves leads to significant enhancement in the intensity of electrons above 1 MeV in the middle magnetosphere. Radial diffusion is capable of transporting MeV electrons accelerated by outer-belt whistler-mode waves into the $M < 10$ region, where they are further accelerated adiabatically to energies of about 10 MeV.

Plain Language Summary To sustain the most intense electron radiation belt in our solar system, Jupiter's magnetosphere needs to pre-accelerate electrons to the energy level of multi-MeV outside the orbit of Io. How such "seed electrons" of the synchrotron radiation belt are effectively accelerated is a challenging question. Gyro-resonance between electrons and whistler-mode waves is believed to be a potential candidate for such pre-acceleration process. In this study, the efficiency of particle acceleration driven by Jovian whistler-mode waves is quantitatively evaluated. With the quasilinear scattering rate calculated with the updated Jovian whistler-mode wave model derived from Juno measurements, 3-D diffusion simulations show that whistler-mode waves between 5 and 25 R_J are capable of accelerating electrons upto about 10 MeV in tens of days. The recently discovered outer whistler-mode belt is found to contribute to the acceleration of multi-MeV electrons.

1. Introduction

The intrinsic magnetic field of Jupiter traps the most intense electron radiation belt in the solar system. In the inner magnetosphere ($M < 5$, following the definition in S. J. Bolton et al. (2004), where M denotes the M-shell of the Jovian magnetic field), synchrotron radiation measurements suggest the presence of ultrarelativistic electrons with energy up to 50 MeV (S. Bolton et al., 2002; de Pater & Dunn, 2003). How such an intense electron belt is generated and sustained has been a long-standing question. As whistler-mode waves are suppressed inside the orbit of moon Io ($M \approx 5.9$) (Menietti et al., 2016), the formation of an intense electron population in the inner magnetosphere is believed to be dominated by inward radial diffusion (de Pater & Goertz, 1990, 1994; Santos-Costa & Bourdarie, 2001). However, such an explanation requires an abundant "seed electron" population (>1 MeV) outside the orbit of Io, which is well above the energy range and intensity level that interchange injections (R. Thorne et al., 1997) or other injection events (Mauk et al., 1999) could provide. In other words, electrons must be pre-accelerated to multi-MeV in the Jovian middle magnetosphere ($5 < M < 30$) to provide sufficient seed populations for the inner radiation belt.

Horne et al. (2008) suggested that the wave-particle interactions between whistler-mode waves and electrons beyond Io may be a potential mechanism that accelerates the existing electron population to the energy of seed electrons. The efficiency of such a process has been investigated by multiple numerical studies in the regime of

both test-particle (e.g., Kubota & Omura, 2018; Tao et al., 2012) and quasilinear diffusion simulations (e.g., Ma et al., 2020; Shprits et al., 2012; E. Woodfield et al., 2013; E. E. Woodfield et al., 2014).

Whistler-mode waves are known to play a dual role in the radiation-belt dynamics at Earth and gas giants. On the one hand, whistler-mode waves are capable of driving fast acceleration of electrons up to multi-MeV at Earth (e.g., Allison et al., 2021; Shprits et al., 2006), Saturn (e.g., E. E. Woodfield et al., 2019; E. Woodfield et al., 2022), and Jupiter (e.g., Horne et al., 2008; Shprits et al., 2012). On the other hand, whistler-mode waves can also drive electron precipitation into the atmosphere and henceforth contribute to the loss of energetic particles at Earth (e.g., Ni et al., 2014; R. M. Thorne et al., 2016; Li et al., 2015; Zhao, Ni, et al., 2019), Saturn (e.g., Kumari et al., 2019; Tripathi et al., 2013), and Jupiter (e.g., Li et al., 2017, 2021; Xiao et al., 2003). To quantitatively investigate the efficiency of wave-particle interactions in providing the seed electrons for the Jovian inner electron belt, a comprehensive numerical simulation for the middle magnetosphere is needed. As the net effect of wave-particle interactions strongly dependent on the initial distribution of electrons (Huang et al., 2018; Shprits et al., 2012; de Soria-Santacruz et al., 2017), 3-D simulations including radial diffusion can be more reliable than 2-D simulations as they could constrain a more realistic distribution of electrons in both the energy and pitch angle dimensions. 3-D simulations also help to understand the possible inward transport (and therefore being additionally accelerated due to the conservation of their first adiabatic invariant) after electrons' being accelerated locally by whistler-mode waves, which has been studied in Earth's outer radiation belt (Liu et al., 2018; Zhao, Baker, et al., 2019). A realistic global model for Jovian whistler-mode waves with M-shell, latitude, and frequency dependence is required for such 3-D simulations. Shprits et al. (2012) also suggested that the latitudinal distribution of waves is of crucial importance in the net effect of whistler-mode waves. Previous studies using the whistler-mode wave profile from Galileo observations (Horne et al., 2008; E. E. Woodfield et al., 2014; de Soria-Santacruz et al., 2017) could possibly have overestimated the net acceleration by whistler-mode waves due to the lack of high-latitude Jovian wave measurements before the Juno mission.

In this paper, we perform 3-D Fokker-Planck simulations for the radial diffusion and local scattering (hereafter referred to as diffusion processes in the dimensions of energy, pitch angle and mixed diffusion terms) by whistler-mode waves of Jovian energetic electrons in the middle magnetosphere to investigate the pre-acceleration of seed electrons. The most updated empirical model for Jovian whistler-mode waves derived from measurements sampled during the first 45 orbits of Juno is used to quantify the scattering rate of electrons.

2. Scattering Rate of Electrons by Whistler-Mode Waves

To quantify the local scattering of electrons by whistler-mode waves in the Jovian magnetosphere, both the spatial distribution of wave intensity and the wave frequency spectrum are needed. Regarding the spatial distribution of the whistler-mode wave intensity, statistical results derived from measurements taken by the Juno spacecraft during its PJ01-PJ45 orbit have been detailed in a companion article (Hao et al., 2024). The survey of whistler-mode wave data covers $5 \le M \le 25$ and $|\lambda| \le 36°$, where λ denotes the magnetic latitude. In the companion article, a novel double-belt distribution of whistler-mode wave is revealed. Figure S1 in Supporting Information S1 presents the mean whistler-mode intensity as a function of M-shell and $|\lambda|$. An outer whistler-mode belt peaking at $M \approx 21$ shows wave intensity over an order of magnitude higher than the slot region ($M \approx 14$), which compels us to study its contribution toward the Jovian electron dynamics.

Regarding the frequency spectrum, we follow the data processing methodology described in Menietti et al. (2021) and extend the data set of statistics with the Juno Extended Mission (PJ34-PJ45) (c.f. Figure 2a in Menietti et al., 2023). According to the spatial distribution of the wave intensity, the data set is divided into four individual regions in the (M, λ) space by $M = 13$ and $|\lambda| = 16°$ (see regions divided by dashed lines in Figure S1 of Supporting Information S1). Within each region, the mean squared wave spectra are derived by

$$\log_{10}\langle B_{Wi}^2 \rangle = \log_{10}\langle \int_{f_{ceq}(\beta_i - \frac{1}{2}\Delta\beta)}^{f_{ceq}(\beta_i + \frac{1}{2}\Delta\beta)} PSD(f_{ceq}\,\beta) f_{ceq}\,d\beta \rangle, \tag{1}$$

where $\langle B_{Wi}^2 \rangle$ denotes the mean squared wave intensity with in each frequency bin ($i = 1, 2, 3 \ldots 8$). $PSD(f)$ denotes the magnetic Power Spectral Density (PSD) at the given frequency f measured by the Waves instrument onboard Juno (Kurth et al., 2017). $\beta = f/f_{ceq}$ is the normalized wave frequency, where f_{ceq} is the electron
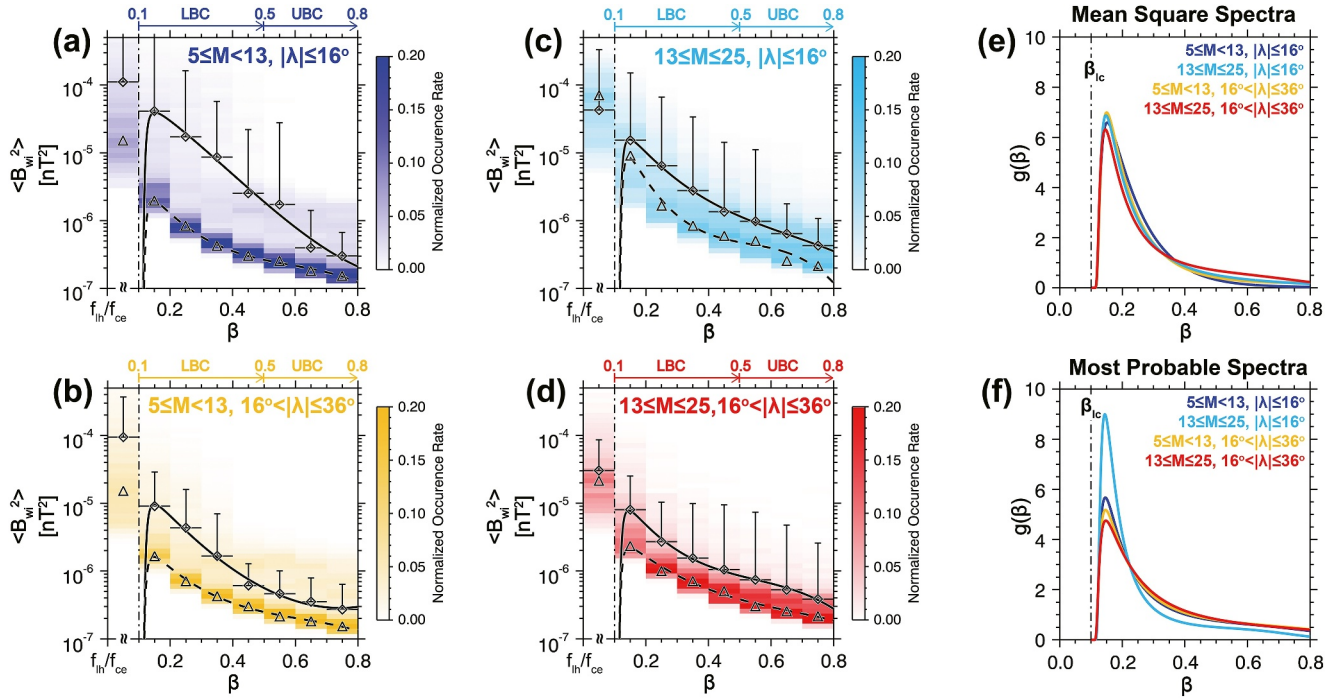
Figure 1. Statistical frequency spectrum of whistler-mode waves. Panel (a) presents the wave intensity distribution measured by the Juno spacecraft in the inner whistler-mode belt ($5 \leq M < 13$) at low magnetic latitude ($|\lambda| > 16°$). The color denotes the probability of wave intensity in each frequency bin. Diamonds denote the average value in each frequency bin and vertical error bars denote their standard error. Triangles denote the most probable value in each frequency bin. Solid and dashed curves show their best polynomial fit within $0.1 < \beta < 0.8$. Lower Band Chorus (LBC) denotes the frequency range from $0.1 f_{ceq}$ to $0.5 f_{ceq}$ while Upper Band Chorus (UBC) denotes the frequency range from $0.5 f_{ceq}$ to $0.8 f_{ceq}$. Panel (b, c, and d) are in the same format as (a) but for high-latitude inner whistler-mode belt, low-latitude outer whistler-mode belt, and high-latitude outer whistler-mode belt, respectively. Panel (e) presents normalized mean square spectra in the aforementioned regions. Panel (f) presents the most probable spectra.

cyclotron frequency at the magnetic equator calculated from the JRM09 + CAN model (Connerney et al., 1981, 2018).

Panels (a–d) of Figure 1 show the statistics for wave frequency spectra in different regions of the Jovian magnetosphere. In addition to the mean squared spectra, the possibility distribution of B_{Wi}^2 and the most probable spectra are also presented. We note that the most probable wave intensity integrated between f_{lh} (lower hybrid frequency) and $0.1 f_{ceq}$ is approximately an order of magnitude higher than that in each frequency bin above $0.1 f_{ceq}$. The statistical wave intensity below $0.1 f_{ceq}$ is likely to be contaminated by other plasma wave modes or noise. Therefore, in this study, we focus on the frequency range $0.1 f_{ceq} < f < 0.5 f_{ceq}$, which is typical for lower-band whistler-mode chorus waves. This lower frequency cutoff at $0.1 f_{ceq}$ is a normal treatment for chorus waves (e.g., Meredith et al., 2012; Wang et al., 2019). As the diffusion coefficients are calculated under the quasilinear assumption, the contribution of plasma waves outside this frequency range (i.e., Z-mode waves or kinetic Alfvén waves, chorus and hiss waves below $0.1 f_{ceq}$) can be easily taken into account by adding their diffusion coefficients to our results once their wave mode and propagation are identified in further studies. The least squares polynomial fit is performed for $\log_{10}\langle B_{Wi}^2 \rangle$ as a function of β in the following form.

$$\log_{10}\langle B_{Wi}^2 \rangle = h(\beta_i) = Q_0 + Q_1\beta_i + Q_2\beta_i^2 + Q_3\beta_i^3 - Q_4(\beta_i - \beta_{lc})^{-3}, \; \beta \geq 0.1. \tag{2}$$

As discussed above, we set $\beta_{lc} = 0.1$ as the lower cutoff of the wave frequency spectra. Here, $Q_{0,1,2,3}$ are free parameters and Q_4 is determined by

$$\frac{dh(\beta)}{d\beta}\Big|_{\beta=0.15} = 0. \tag{3}$$
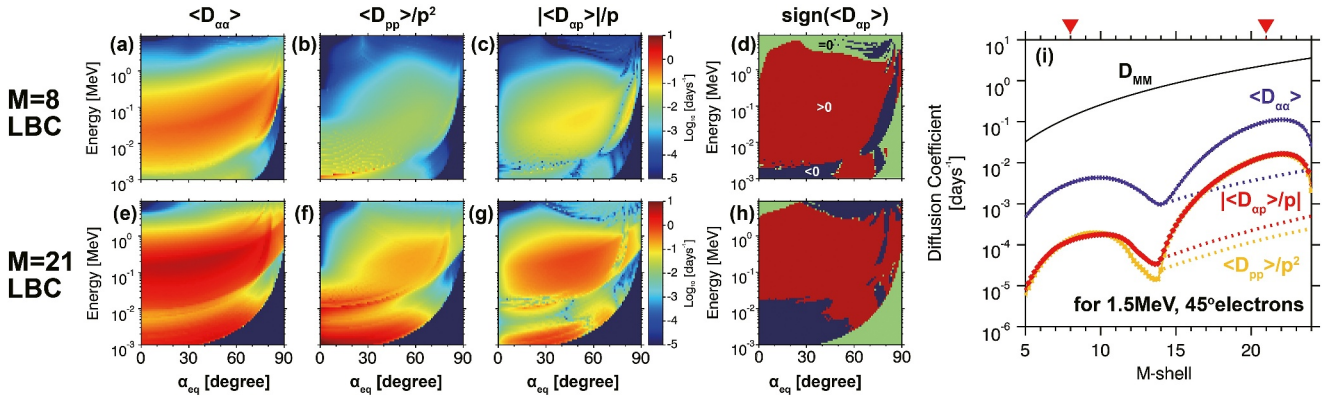
Figure 2. Diffusion coefficients of electrons scattered by Jovian whistler-mode waves in LBC frequency range. (a–d): pitch angle, energy (momentum), mixed scattering rate and sign of mixed scattering rate in the inner whistler-mode belt ($M = 8$). (e–h): same format but calculated in the outer whistler-mode belt ($M = 21$). Panel (a–c) and (e–g) share the same vertical coordinate axises. (i): diffusion coefficients for 1.5 MeV, $\alpha_{eq} = 45°$ electrons driven by whistler-mode waves in the frequency range of lower band chorus as a function of the M-shell. Dashed curves show the case that the outer whistler-mode belt is artificially suppressed. Black curve gives a typical profile of radial diffusion rate in Jovian magnetosphere.

Then the normalized frequency distribution function $g(\beta)$ can be defined as

$$g(\beta) = \frac{10^{h(\beta)}}{\int_{lc}^{uc} 10^{h(\beta)} \, d\beta} = \frac{10^{h(\beta)}}{G_0}. \tag{4}$$

The fitting results for both the mean squared spectra and the most probable spectra of the whistler-mode waves are overplotted in Figures 1a–1d. Their normalized distribution functions $g(\beta)$ are shown in Figures 1e and 1f. In this study, region-specific $g(\beta)$ functions derived from mean squared spectra are used to calculate the diffusion coefficients of whistler-mode waves. As there is not much difference between the normalized frequency distribution function for the mean squared wave spectrum fitted from each different spatial region, we suggest that it might also be feasible to use a single $g(\beta)$ function for the entire spatial volume.

Figure 2 presents the phase-averaged diffusion coefficients (averaged among the gyration, bounce and drift phase of electrons) calculated with the Full Diffusion Code (FDC) (Ni et al., 2008; Shprits & Ni, 2009), which is based on the quasilinear formulations detailed in Glauert and Horne (2005) and J. Albert and Young (2005). The M-shell and latitude dependence of the wave intensity are adapted from the companion study on the spatial distribution of whistler-mode waves (Hao et al., 2024; Figure 2). The normalized power spectrum density $g(\beta)$ of the whistler-mode waves shown in Figure 1e is used. In this study, we set a fixed cutoff $f_{lc} = 0.1 f_{ceq}$ and $f_{uc} = 0.5 f_{ceq}$ of the frequency distribution to study the contribution of whistler-mode waves in the frequency range of the Lower Band Chorus (LBC) wave. The distribution of the wave normal angle θ centered in the field-aligned direction is also assumed. A Gaussian distribution of $X = \tan(\theta)$ centered at $\theta_m = 0°$ with width $\delta\theta = 30°$ and cutoff at $\theta_{uc} = 70°$ is used to calculate the coefficients, which are the same parameters as Shprits et al. (2012) and de Soria-Santacruz et al. (2017). Landau resonance ($n = 0$) and the gyroresonance ($n = \pm1, \pm2, \ldots, \pm5$) are taken into account. For simplicity, we use the plasma density profile $N_e = 3.2 \times 10^8 M^{-6.9} \text{cm}^{-3}$ (Frank et al., 2002) without latitude dependence and a dipole magnetic field model in the diffusion coefficient calculation.

Panel (i) of Figure 2 presents the M-shell dependence of the local diffusion coefficients. The bounce-averaged pitch angle scattering rate ($\langle D_{\alpha\alpha} \rangle$) of $E_k = 1.5$ MeV, $\alpha_{eq} = 45°$ electrons varies from $5 \times 10^{-3} \text{days}^{-1}$ to $4 \times 10^{-2} \text{days}^{-1}$ among $5 < M < 25$. The kinetic energy of the electrons E_k equals $\sqrt{p^2c^2 + m_0^2c^4} - m_0c^2$, where m_0 denotes the rest mass of the electrons and c denotes the speed of light. For (1.5 MeV, 45°) electrons, $\langle D_{\alpha\alpha} \rangle$ is approximately one order of magnitude higher than momentum scattering ($\langle D_{pp} \rangle/p^2$) and mixed pitch angle-momentum ($|\langle D_{\alpha p} \rangle/p|$) scattering, while the momentum and mixed scattering rate are comparable. The local scattering rates peak at $M \approx 8$ and $M \approx 21$, corresponding to the double-belt structure of statistical whistler-mode wave intensity (Hao et al., 2024). Local diffusion coefficients as a function of E_k and α_{eq} in the heart of the inner and outer whistler-mode belt ($M = 8$ and $M = 21$, respectively) are shown in Figures 2a–2h.

The radial diffusion coefficient (D_{MM}) is also compared with the local scattering rate. We use the formula $D_{MM} = D_0 \cdot M^n$ for radial diffusion (Schulz & Lanzerotti, 1974). For simplicity, the dependence of energy and pitch angle on radial diffusion is not taken into account. $n = 3$ and $D_0 = 3 \times 10^{-9} \mathrm{s}^{-1}$ are typical values for electrons around Jupiter (de Pater & Goertz, 1994), which is used by both E. E. Woodfield et al. (2014) and this study in Fokker-Planck diffusion simulations. As marked by the black curve in Figure 2i, the radial diffusion coefficient is more than an order of magnitude higher than all the local diffusion coefficients of the (1.5 MeV, 45°) electrons.

In order to quantify the effect of the lately discovered outer whistler-mode belt on electron dynamics, we also attempt to evaluate the local scattering rates in the case that the outer whistler-mode belt did not exist. In a second set of FDC calculations, we set the whistler-mode wave intensity at $M > 14$ to be the same value as $M = 14$, where the wave intensity is around an order of magnitude weaker than at the heart of the inner or outer whistler-mode belt. Other input parameters for the FDC code remain the same as aforementioned. The dashed curves in Figure 2i show the scattering rates for the case where the outer whistler-mode belt was removed. Among $14 < M < 25$, the local diffusion coefficients are significantly suppressed (by over an order of magnitude at $M \approx 21$) and increase monotonically with the radial distance.

3. VERB 3-D Simulations of Local Scattering and Radial Diffusion

To quantitatively evaluate the effect of local scattering by Jovian whistler-mode waves, we perform 3-D numerical simulations with the Versatile Electron Radiation Belt (VERB) diffusion code (Shprits et al., 2006; Subbotin & Shprits, 2009; Subbotin et al., 2010), in which a fully implicit numerical scheme is used to solve the modified Fokker-Planck equation (i.e., Schulz & Lanzerotti, 1974)

$$
\begin{aligned}
\frac{\partial f}{\partial t} = & M^2 \frac{\partial}{\partial M}\bigg|_{\mu,K} \left(\frac{1}{M^2} D_{MM} \frac{\partial}{\partial M}\bigg|_{\mu,K} f \right) \\
& + \frac{1}{p^2} \frac{\partial}{\partial p}\bigg|_{\alpha,M} p^2 \left(\langle D_{pp} \rangle \frac{\partial}{\partial p}\bigg|_{\alpha,M} f + \langle D_{p\alpha} \rangle \frac{\partial}{\partial \alpha}\bigg|_{p,M} f \right) \\
& + \frac{1}{T(\alpha)\sin(2\alpha)} \frac{\partial}{\partial \alpha}\bigg|_{p,M} T(\alpha)\sin(2\alpha) \\
& \cdot \left(\langle D_{\alpha\alpha} \rangle \frac{\partial}{\partial \alpha}\bigg|_{p,M} f + \langle D_{\alpha p} \rangle \frac{\partial}{\partial p}\bigg|_{\alpha,M} f \right) - \frac{f}{\tau},
\end{aligned}
\tag{5}
$$

where f is the fully phase-averaged Phase Space Density (PhSD, to differentiate it from the power spectral density of waves) of the electrons (averaged over the gyration, bounce and drift phase of electrons), t is the simulation time. p and α (also used as α_{eq} hereafter) denote the relativistic momentum and the equatorial pitch angle of the electrons. μ, K and M ($M = M^*$ in the dipole field) denote the first (gyration), second (bounce), and third (drift) adiabatic invariant of electrons. D_{MM}, $\langle D_{pp} \rangle$, $\langle D_{\alpha\alpha} \rangle$ and $\langle D_{\alpha p} \rangle (\equiv \langle D_{p\alpha} \rangle)$ are the coefficients of radial, bounce-averaged momentum, pitch angle and mixed diffusion discussed in Section 2. τ is the lifetime of electrons, which is defined as infinite outside the loss cone and as a quarter of the bounce period inside the loss cone. $T(\alpha)$ is a non-dimensional function for particles' bounce motion in a dipole field (detailed in Equation 19 of Lenchek et al. (1961)).

3.1. Grids, Boundary and Initial Conditions

In this paper, we simulate the PhSD evolution of electrons up to 30 MeV at the spatial extent of $1 \leq M \leq 25$. $(201 \times 91 \times 121)$ grids in the (E_k, α, M) space are used. Detailed setup of the grids is described in Text S1 of Supporting Information S1.

Similar boundary conditions to most VERB-3D simulations for the terrestrial radiation belt (e.g., Subbotin & Shprits, 2009) are adapted for simulations in this paper, but with electron spectra from the GIRE2 model (de Soria-Santacruz et al., 2016). The setup of the boundary conditions is detailed in Text S2 of Supporting Information S1.
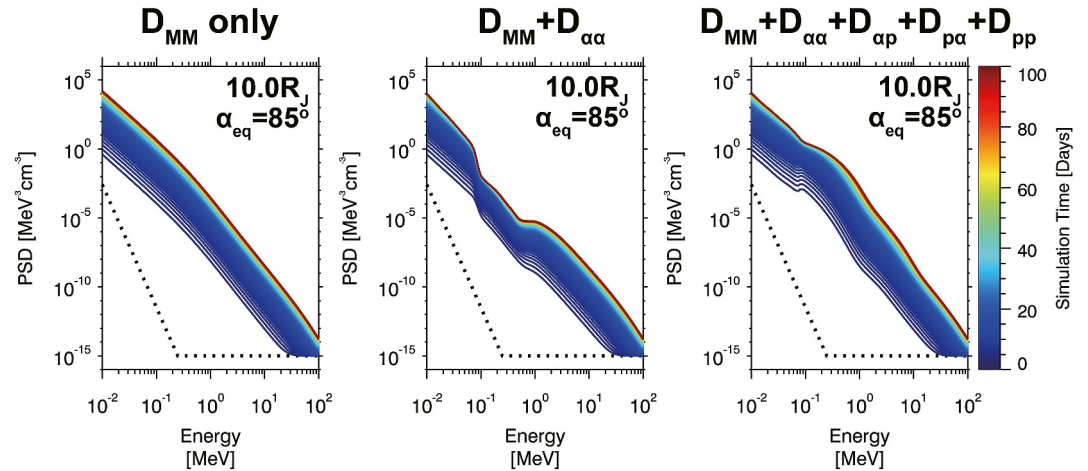
Figure 3. The evolution of Jovian electron energy spectrum during the 100 days of Fokker-Planck simulations. Color-coded curves show the energy spectra at different simulation time at $10\,R_J$. Dashed curves show the initial condition of the simulations. The left panel shows the simulation with only radial diffusion included. The middle panel shows the simulation with radial diffusion and pitch angle scattering included. The right panel shows the simulation with radial diffusion and all local diffusion terms included.

The net effect of wave-particle interactions in 2-D Fokker-Planck simulations strongly depends on the initial conditions (e.g., Huang et al., 2018). When simulation the whistler-mode-driven Jovian radiation belt dynamics, Horne et al. (2008) propagated electron distribution at $15.75R_J$ adiabatically to $10R_J$ and initiated 2-D diffusion. As to the initial condition for 3-D Fokker-Planck simulations, we start our runs with an "empty magnetosphere", in which no pre-existing MeV electrons are included in the system. Whistler-mode waves immediately scatter the electrons propagated inward by radial diffusion from the outer boundary in M-shell. The initial condition is an input in the radial diffusion grid in the VERB code. For each specific (μ, k) value, background-level electron PhSD is set for the 61st to 201th grids in the E_k dimension. A soft power law spectrum $f(E_k) = f_{lc} \cdot \left(\frac{E_k}{E_{lc}}\right)^{-\lambda}$ linking the boundary E_k and the 61st grid gives the PhSD value for the second to 60th E_k grids (for the 60th grid in energy dimension, $E_k \approx 120\,\text{keV}$ at $M = 10$), where f_{lc} comes from the boundary condition at $E_k = E_{lc}$. The dotted curves in Figure S1 of Supporting Information S1 show the initial energy spectrum at $M = 10$. The previous numerical study used a similar form of initial condition and showed that the softness of the initial spectrum has a very limited effect on the results of 2-D local diffusion simulations (E. E. Woodfield et al., 2014, Figure 9). Such an "empty magnetosphere" initial condition enables us to start our simulations with a Jovian magnetosphere containing no pre-existing MeV electrons and investigate how the MeV-electron population is built and shaped by radial transport and local processes.

3.2. Acceleration and Loss Driven by Whistler-Mode Waves

Figure 4 presents a comparison among three individual simulations in which different terms of local diffusion are included. The ratios among spectra presented in Figures 4a–4d are shown in Figures S2a–S2d of Supporting Information S1. The initial and boundary conditions used in these simulations are identical to each other. The time evolution of the simulated PhSDs is shown in Figure 3, indicating that the systems of the three simulations mentioned above have evolved to their quasistatic states after 100 days. After 100 days of evolution, the simulation in which both pitch angle scattering and radial diffusion are included shows a significantly lower PhSD in comparison to the case where only radial diffusion is taken into account and all other loss and source processes are neglected. As shown in Figure 4e (see also dotted curves in Figure S2 of Supporting Information S1 for the PhSD ratio), pitch angle scattering by whistler-mode waves leads to a significant loss of electrons by more than an order of magnitude over a wide range of M-shells and values of kinetic energy. As the M-shell decreases from 20 to 5, the upper edge in E_k of the region with significant PhSD depletion extends from ~ 2 to $\sim 10\,\text{MeV}$. This curve in (M, E_k) appears to approximately follow a constant first adiabatic invariant, indicating a synergy of loss by local pitch-angle scattering and radial diffusion.
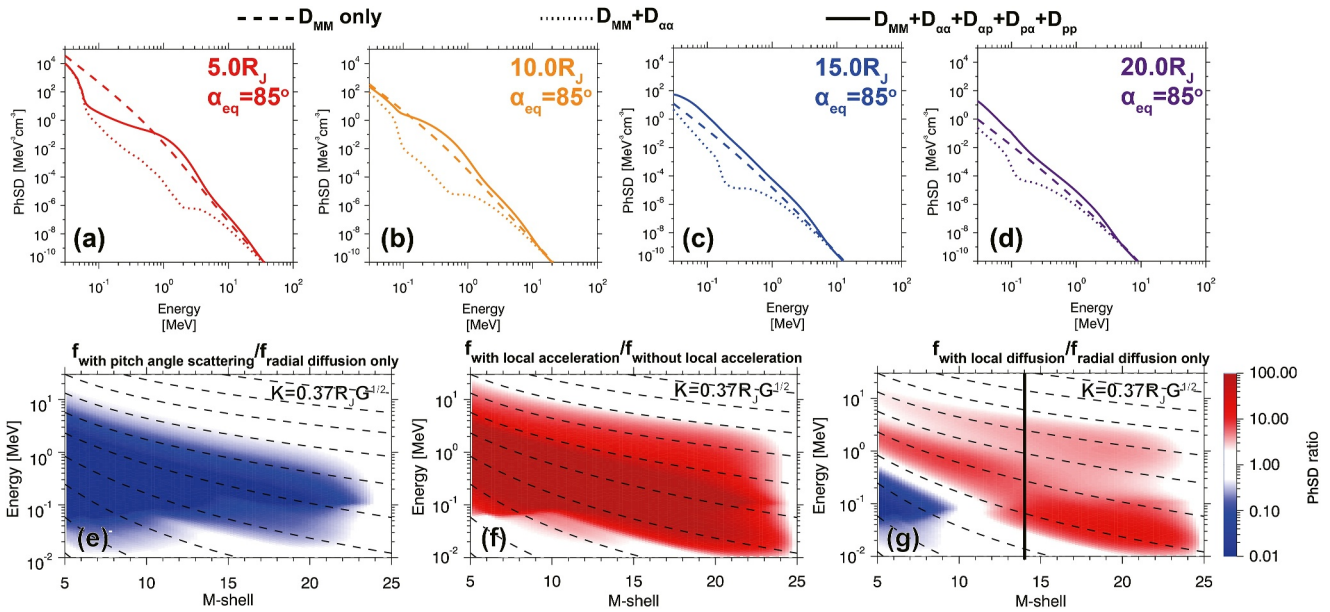
Figure 4. Electron energy spectrum after 100 days of Fokker-Planck simulations starting from an empty magnetosphere. Panel (a–d) show the results for near-equator mirroring electrons at 5, 10, 15 and 20 R_J. Solid curves show results with all diffusion terms involved. Dotted curves show the results simulated with radial diffusion and pitch angle scattering. Dashed curves show the case in which only radial diffusion is considered. Panel (e) depicts the comparison between phase space density profiles simulated with and without pitch angle scattering. Dashed curves trace the electron energy with a set of constant first adiabatic invariants. Panel (f) is in the same format but depicts the effect of energy (momentum) and mixed diffusion terms. Panel (g) is also in the same format but depicts the net effect of all local diffusion terms by whistler-mode waves in LBC frequency. Vertical dashed line indicates the separation M-shell between inner and outer whistler-mode belt.

Figure 4f (see also the dashed curves in Figure S2 of Supporting Information S1) presents the contribution of local acceleration ("D_{pp}", "$D_{p\alpha}$" and "$D_{\alpha p}$"). When momentum and mixed pitch angle-momentum diffusion is included, the PhSD of electrons increases by an order of magnitude in comparison with the case of radial plus pitch angle diffusion ("$D_{MM} + D_{\alpha\alpha}$") in a broad range of energy after 100 days of evolution. At $M = 5$ and $M = 10$, the increase in PhSD for 1 MeV electrons exceeds two orders of magnitude. This demonstrates that momentum and mixed diffusion contribute significantly to the acceleration of electrons from 100 keV to several MeV.

Figure 4g evaluates the net effect of whistler-mode waves on building the electron population in the Jovian middle magnetosphere. Including all local diffusion terms, namely $D_{\alpha\alpha}$, D_{pp}, $D_{p\alpha}$, and $D_{\alpha p}$, results in a higher PhSD for energies from 10 keV to 2 MeV at $14 < M < 25$. At $M < 14$, the zone of net increase in PhSD extends to the multi-MeV range, following constant curves μ. PhSD depletion is evident for energies from 10 to 100 s keV at $M < 10$. Such differences indicate a complicated competition between acceleration and loss driven by whistler-mode waves and their dependence on M-shells. The outer whistler-mode belt predominantly accelerates electrons. Electrons accelerated by the outer whistler-mode belt are further transported into the lower M-shell, during which they get adiabatically accelerated to multi-MeV level (discussed in detail in Section 3.4). The inner whistler-mode belt is efficient in driving the atmospheric loss of sub-MeV electrons by scattering them into the loss cone. As the result, the net effect of the whistler-mode waves throughout the middle magnetosphere toward electrons is energy dependent in our simulations. For >1 MeV electrons, acceleration compensates for and outweighs loss, leading to a considerable increase in PhSD (by a factor of 8 for 2 MeV electrons at $M = 5$).

3.3. Importance of Mixed Diffusion

Figure 5 compares the simulations that include and exclude the mixed pitch angle-energy diffusion terms ("$D_{\alpha p}$" and "$D_{p\alpha}$"). 3-D simulation without mixed terms gives similar "flat top" PAD of multi-MeV electrons as the previous 2-D simulation results without mixed terms (see Horne et al., 2008, Figure 4b), which is not recorded in the measurement by Galileo-EPD (Nénon et al., 2022). "Flat-top PAD" is no longer visible in the simulation results when mixed diffusion is taken into account. As shown in Figure S2 of Supporting Information S1, the PhSD of MeV electrons with a pitch angle close to 90° evolving under full diffusion terms could be an order of
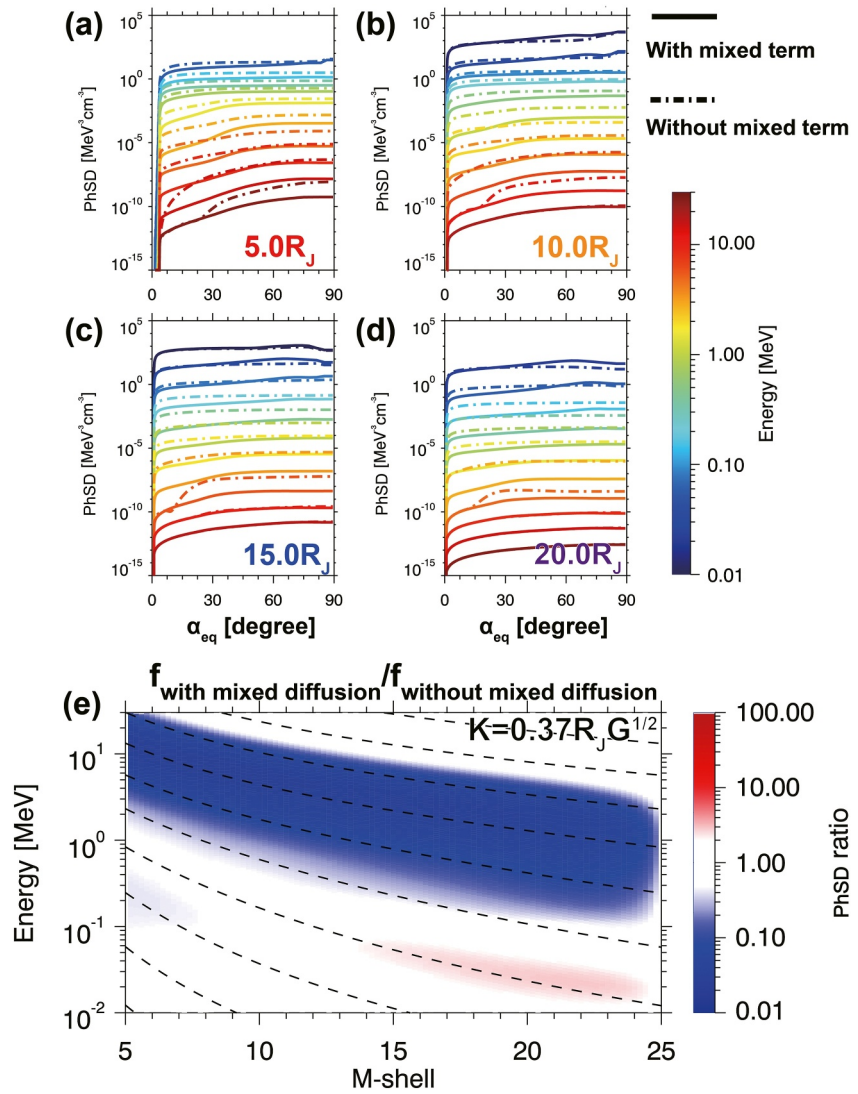
Figure 5. Evaluating the effect of mixed diffusion terms. Panel (a–d) present the pitch angle distribution of electrons at 5, 10, 15 and 20 R_J after 100 days of evolution from an empty magnetosphere. Solid (dash-and-dot) curves show the simulation results with (without) mixed diffusion curves. Color of each curve denotes the energy of electrons. Panel (e) is in the same format as Figure 3e but compares the results with and without mixed diffusion term.

magnitude lower than without mixed terms after 100 days of simulation. Omitting the mixed terms could result in a significant overestimation of the acceleration of the Jovian multi-MeV electron population, which is consistent with the effect of mixed terms of chorus scattering in the outer radiation belt of Earth (J. Albert & Young, 2005; J. M. Albert et al., 2009; Subbotin et al., 2010; Su et al., 2011; Tao et al., 2009; Xiao et al., 2010).

3.4. Contribution of the Outer Whistler-Mode Belt

Measurements taken by Juno during its first 45 orbits have revealed a second belt of whistler-mode wave emission peaking at $M \approx 21$ (Hao et al., 2024). To examine the effect of such an outer whistler-mode belt on energetic electrons, we run an additional 3-D VERB simulation, in which the outer whistler-mode belt is artificially removed. The local diffusion coefficients used in this simulation are discussed in Section 2 (see the dashed curves in Figure 2i). Radial, momentum, pitch angle, and mixed diffusion processes have been taken into account. Figure 6 presents the comparison between the full 3-D diffusion results with and without the outer whistler-mode belt. At the heart of the outer whistler-mode belt ($M = 21$), the simulation with the outer whistler-mode belt gives PhSD larger than without the outer whistler-mode belt from 10 keV to 3 MeV. In the inner whistler-mode belt
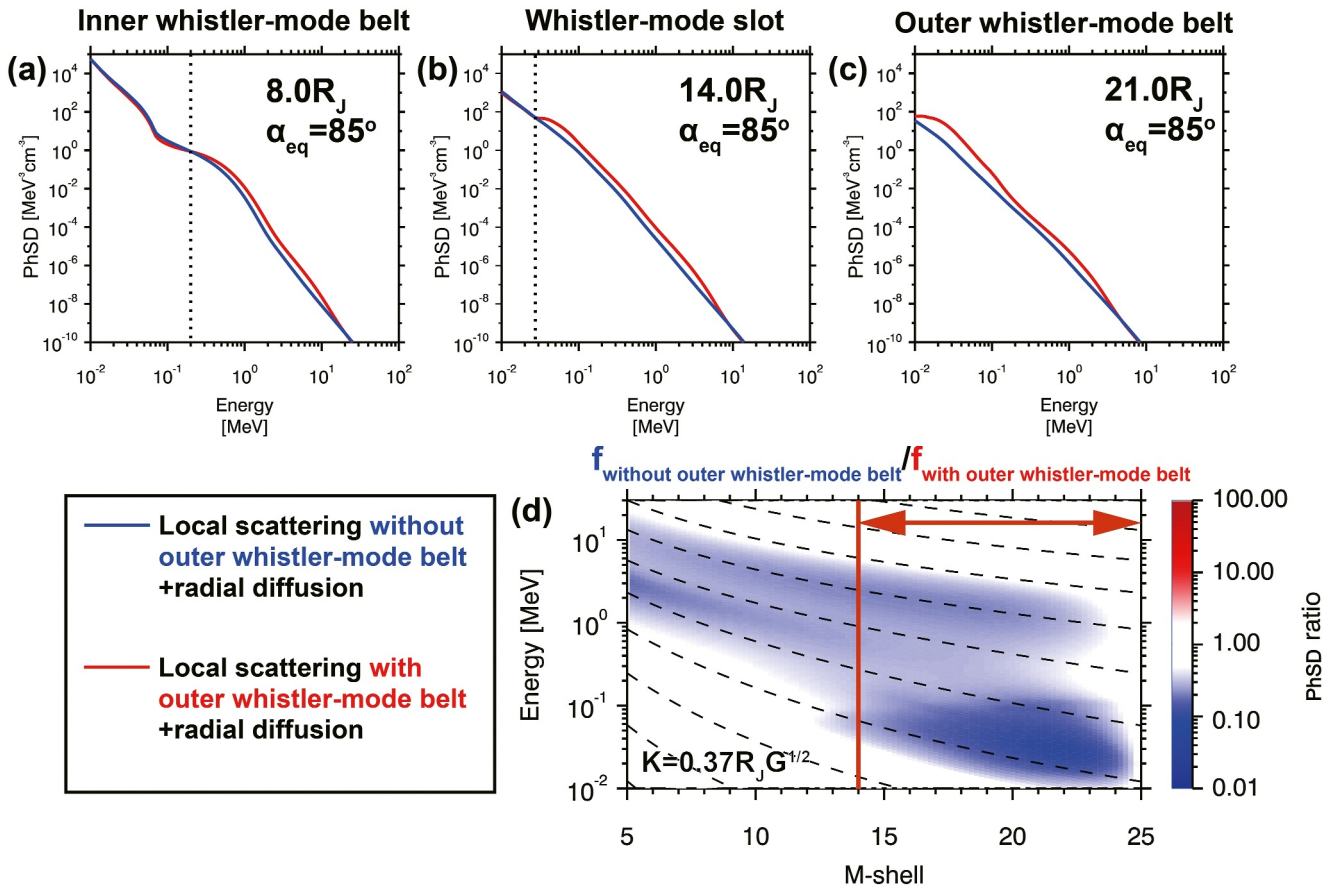
Figure 6. Evaluating the contribution of outer whistler-mode belt. Panel (a–c) show electron energy spectrum in the inner whistler-mode belt ($M = 8$), slot region of wave intensity ($M = 14$) and the outer whistler-mode belt ($M = 21$). Blue curves show the VERB 3D diffusion results after 100 days for the case that the outer whistler-mode belt is artificially suppressed while red curves show the case that the outer whistler-mode belt is included. Dashed vertical lines mark the threshold energy where the simulation with outer whistler-mode belt gives stronger electron phase space density. Panel (d) compares the results without and with the outer whistler-mode belt in the same format as Figure 3e. Red vertical line and arrows mark the M-shell extent where whistler-mode wave intensity is artificially suppressed.

($M = 8$), the energy range of PhSD enhancement due to the outer whistler-mode belt starts at 200 keV and extends to above 10 MeV. The comparison between simulated PhSD profiles that exclude and include the outer whistler-mode belt is shown in Figure 6d (see Figure S3 in Supporting Information S1 for line plots). For an electron population below 200 keV, the effect of the outer whistler-mode belt is around an order of magnitude in the electron PhSD but mostly confined in the region of $M > 14$. For an electron population above 100 keV, the net effect of the outer whistler-mode belt is weaker (by a factor of 3–5 in PhSD for $1 < E_k < 10$ MeV electrons at $M = 8$), but spatially continuous between $5 < M < 23$. The upper energy limit of electrons affected by the outer whistler-mode belt in the (M, E_k) space follows a curve of constant μ. We suggest that in our simulations electrons above 200 keV get accelerated locally by the outer-belt whistler-mode waves and then transported inward adiabatically by radial diffusion. Cooperation between the local acceleration of the outer whistler-mode belt (synchrotron acceleration) and the inward radial transport (betatron acceleration) adds to the multi-MeV electron population inside 14 R_J.

4. Summary and Discussion

In this study, we have evaluated the effect of whistler-mode waves toward energetic electrons in the Jovian middle magnetosphere. Through comparison among Fokker-Planck simulation results with various sets of local diffusion coefficients, we could draw the following conclusions.

1. Whistler-mode waves between $0.1f_{ceq}$ and $0.5f_{ceq}$ in the middle magnetosphere contribute to considerable acceleration of Jovian multi-MeV electrons (by around a factor of five in simulated PhSD), which are of the right energy to sustain the ultrarelativistic inner radiation belt.

2. Mixed diffusion terms are important in evaluating the wave-particle interactions between Jovian electrons and whistler-mode waves. Fokker-Planck simulation without pitch angle-energy diffusion terms overestimates the acceleration of Jovian MeV electrons by whistler-mode waves.

3. Intense whistler-mode waves outside $M = 15$ recently observed by Juno do contribute to the acceleration of Jovian electrons in a wide range of M-shell and energy. Radial diffusion is capable of transporting the MeV electrons accelerated by the outer whistler-mode belt into the $M < 10$ region and further accelerate them adiabatically upto 10 MeV.

In Section 3.4, comparison between the simulated electron phase space density with and without the outer whistler-mode belt indicates a two-step process for Jovian electrons to accelerate up to the 10 MeV range. Electrons accelerated by the outer whistler-mode belt can be further adiabatically energized by radial transport processes, which is similar to the mechanism proposed by Liu et al. (2018) and Zhao, Baker, et al. (2019) for terrestrial outer belt electrons. The chance for electrons to get locally accelerated at a larger M-shell (namely in the outer whistler-mode belt) significantly increases the efficiency of the middle magnetosphere as a "pump" for the ultrarelativisitc inner radiation belt.

Kollmann et al. (2018) analyzed the upper cutoff energy (E_c) in the electron energy spectrum measured by the EPD instrument onboard the Galileo spacecraft and found an increasing E_c toward Jupiter. The L-shell (or M-shell) dependence of E_c appears to follow a curve along which the first adiabatic invariant is conserved within a wide radial extent, based on which they concluded that adiabatic radial transport is the predominant acceleration mechanism. In our simulation results, the net effect of whistler-mode waves (see Figure 4g), especially the outer whistler-mode belt (see Figure 6d), also shows a similar radial distribution. The upper cutoff energies of net acceleration by whistler-mode waves also follow the curve of constant μ. In other words, the net effect of local acceleration can propagate across a wide range of M-shells by radial diffusion. Therefore, local acceleration by whistler-mode waves along with radial diffusion may also result in a similar profile in $E_c(M)$. The effect of local processes toward multi-MeV electrons may not be easily ruled out by the upper cutoff in the electron energy spectrum.

As discussed in our companion paper (Hao et al., 2024), the outer whistler-mode belt for the wave frequency above $0.1f_{ceq}$ at $14 < M < 25$ is likely to be a mixture of chorus waves originating from the near-equator region and auroral hiss waves generated in the polar region. Differentiating them in a statistical study is difficult. However, the origin of various types of whistler-mode waves does not change the validity of our simulation results. Auroral hiss waves also scatter electrons and have the same dispersion relation as chorus waves. In our study, only the whistler-mode waves sampled within $|\lambda| < 36°$ are taken into account. Therefore, the auroral hiss waves that contribute to the whistler-mode wave model used in this study are most likely to propagate in ducted mode, and therefore their wave normal angle can also not be far away from the field aligned direction. Therefore, our calculation on the scattering rate of electrons in Section 2 applies to either types of whistler-mode waves. Our Fokker-Planck simulation results do not essentially change with the origin of whistler-mode waves.

In this study, statistical frequency spectra of the wave have also been used to derive the scattering rate of electrons, which could be more realistic than Gaussian-like frequency spectra in previous studies on wave-particle interactions in the Jovian magnetosphere (e.g., de Soria-Santacruz et al., 2017; Shprits et al., 2012). The numerical simulations in this study could be improved in several aspects. For simplicity, a dipole field and a constant plasma density along the field line are assumed in our simulations. 2-D simulations by Ma et al. (2020) suggested that the acceleration of multi-MeV electrons is enhanced when realistic density and magnetic models are taken into account. f_{ceq} from JRM + CAN model was used to better constrain the nature of whistler-mode waves while dipole field is used to quantify diffusion coefficients and to run Fokker-Planck simulation, which makes our simulations less self-consistent. In this study, we focus on the wave frequency range $0.1f_{ceq} \sim 0.5f_{ceq}$. As the scattering rates of waves are calculated with the quasilinear method, the scattering rate of the full wave spectrum can be derived in future studies simply by adding the current results to the contribution of the rest of the wave spectrum (e.g., upper band chorus and low-frequency hiss waves). The Juno data used to generate our statistical wave model come from PJ01–45 orbits, during which only the night sector of the Jovian magnetosphere is sampled. In this study, the mean value of the wave intensity in all available MLTs is used to calculate the diffusion coefficients. MLT

dependence of wave emission (especially the day-night asymmetry) is neglected, which awaits accumulation of data from the Juno extended mission and cross calibration with Galileo data. Several physical processes have not been considered in our simulations, such as Coulomb collisions and synchrotron radiation (e.g., Nénon et al., 2017). In reality, the contribution of whistler-mode waves to electron acceleration depends more or less on the efficiency of radial diffusion and its energy dependence. We must note that the radial diffusion coefficient (D_{MM}) for energetic Jovian electrons at $5 \leq M \leq 25$ is not exactly quantitatively known. A better understanding of the radial diffusion coefficient may benefit from investigating the microsignatures and their fading rates of Jovian moons, which is similar to the case of Saturn (e.g., Roussos et al., 2005; Van Allen et al., 1980). In addition, non-diffusive resonant radial transport is also known to contribute to the prompt acceleration of ultrarelativistic electrons in the Jovian magnetosphere (Hao et al., 2020; Roussos et al., 2018). It could be a challenging task for future investigations to conduct a comprehensive simulation using realistic wave, plasma density, and magnetic field models accounting for more physical processes and to compare the simulated energy spectrum, pitch angle distributions, and radial profile of electrons with Galileo/Juno measurements.

Conflict of Interest

Y. Y. S declares a potential conflict of interest and significant financial interest in Space Sciences Innovations Inc. In Seattle, WA.

Data Availability Statement

Juno WAV data can be obtained at https://pds-ppi.igpp.ucla.edu/collection/JNO-E_J_SS-WAV-3-CDR-SRVFULL-V2.0:DATA.

References

Albert, J., & Young, S. (2005). Multidimensional quasi-linear diffusion of radiation belt electrons. *Geophysical Research Letters*, *32*(14). https://doi.org/10.1029/2005gl023191

Albert, J. M., Meredith, N. P., & Horne, R. B. (2009). Three-dimensional diffusion simulation of outer radiation belt electrons during the 9 October 1990 magnetic storm. *Journal of Geophysical Research*, *114*(A9). https://doi.org/10.1029/2009ja014336

Allison, H. J., Shprits, Y. Y., Zhelavskaya, I. S., Wang, D., & Smirnov, A. G. (2021). Gyroresonant wave-particle interactions with chorus waves during extreme depletions of plasma density in the Van Allen radiation belts. *Science Advances*, *7*(5), eabc0380. https://doi.org/10.1126/sciadv.abc0380

Bolton, S., Janssen, M., Thorne, R., Levin, S., Klein, M., Gulkis, S., et al. (2002). Ultra-relativistic electrons in Jupiter's radiation belts. *Nature*, *415*(6875), 987–991. https://doi.org/10.1038/415987a

Bolton, S. J., Thorne, R. M., Bourdarie, S., de Pater, I., & Mauk, B. (2004). Jupiter's inner radiation belts. Jupiter: The Planet. *Satellites, and Magnetosphere*, *1*, 671–688.

Connerney, J., Acuna, M., & Ness, N. (1981). Modeling the Jovian current sheet and inner magnetosphere. *Journal of Geophysical Research*, *86*(A10), 8370–8384. https://doi.org/10.1029/ja086ia10p08370

Connerney, J., Kotsiaros, S., Oliversen, R., Espley, J., Joergensen, J. L., Joergensen, P., et al. (2018). A new model of Jupiter's magnetic field from Juno's first nine orbits. *Geophysical Research Letters*, *45*(6), 2590–2596. https://doi.org/10.1002/2018gl077312

de Soria-Santacruz, M., Garrett, H., Evans, R., Jun, I., Kim, W., Paranicas, C., & Drozdov, A. (2016). An empirical model of the high-energy electron environment at Jupiter. *Journal of Geophysical Research: Space Physics*, *121*(10), 9732–9743. https://doi.org/10.1002/2016ja023059

de Soria-Santacruz, M., Shprits, Y., Drozdov, A., Menietti, J., Garrett, H., Zhu, H., et al. (2017). Interactions between energetic electrons and realistic whistler mode waves in the Jovian magnetosphere. *Journal of Geophysical Research: Space Physics*, *122*(5), 5355–5364. https://doi.org/10.1002/2017ja023975

de Pater, I., & Dunn, D. E. (2003). VLA observations of Jupiter's synchrotron radiation at 15 and 22 GHz. *Icarus*, *163*(2), 449–455. https://doi.org/10.1016/s0019-1035(03)00068-x

de Pater, I., & Goertz, C. K. (1990). Radial diffusion models of energetic electrons and Jupiter's synchrotron radiation: 1. Steady state solution. *Journal of Geophysical Research*, *95*(A1), 39–50. https://doi.org/10.1029/ja095ia01p00039

de Pater, I., & Goertz, C. K. (1994). Radial diffusion models of energetic electrons and Jupiter's synchrotron radiation: 2. Time variability. *Journal of Geophysical Research*, *99*(A2), 2271–2287. https://doi.org/10.1029/93ja02097

Frank, L., Paterson, W., & Khurana, K. (2002). Observations of thermal plasmas in Jupiter's magnetotail. *Journal of Geophysical Research*, *107*(A1), SIA. https://doi.org/10.1029/2001ja000077

Glauert, S. A., & Horne, R. B. (2005). Calculation of pitch angle and energy diffusion coefficients with the PADIE code. *Journal of Geophysical Research*, *110*(A4). https://doi.org/10.1029/2004ja010851

Hao, Y.-X., Shprits, Y. Y., Menietti, J. D., Liu, Z. Y., Averkamp, T., Wang, D. D., et al. (2024). Jupiter's whistler-mode belts and electron slot region. *Journal of Geophysical Research: Space Physics*, *129*, e2024JA032850. https://doi.org/10.1029/2024JA032850

Hao, Y.-X., Sun, Y.-X., Roussos, E., Liu, Y., Kollmann, P., Yuan, C.-J., et al. (2020). The formation of Saturn's and Jupiter's electron radiation belts by magnetospheric electric fields. *The Astrophysical Journal Letters*, *905*(1), L10. https://doi.org/10.3847/2041-8213/abca3f

Horne, R. B., Thorne, R. M., Glauert, S. A., Douglas Menietti, J., Shprits, Y. Y., & Gurnett, D. A. (2008). Gyro-resonant electron acceleration at Jupiter. *Nature Physics*, *4*(4), 301–304. https://doi.org/10.1038/nphys897

Huang, J., Gu, X., Ni, B., Luo, Q., Fu, S., Xiang, Z., & Zhang, W. (2018). Importance of electron distribution profiles to chorus wave driven evolution of Jovian radiation belt electrons. *Earth and Planetary Physics*, *2*(5), 371–383. https://doi.org/10.26464/epp2018035

Kollmann, P., Roussos, E., Paranicas, C., Woodfield, E. E., Mauk, B., Clark, G., et al. (2018). Electron acceleration to MEV energies at Jupiter and Saturn. *Journal of Geophysical Research: Space Physics*, *123*(11), 9110–9129. https://doi.org/10.1029/2018ja025665

Kubota, Y., & Omura, Y. (2018). Nonlinear dynamics of radiation belt electrons interacting with chorus emissions localized in longitude. *Journal of Geophysical Research: Space Physics*, *123*(6), 4835–4857. https://doi.org/10.1029/2017ja025050

Kumari, J., Tripathi, A. K., Singhal, R. P., & Singh, O. N., II. (2019). Investigation of Saturn's aurora by whistler mode waves. *Icarus*, *321*, 251–259. https://doi.org/10.1016/j.icarus.2018.10.015

Kurth, W., Hospodarsky, G., Kirchner, D., Mokrzycki, B., Averkamp, T., Robison, W., et al. (2017). The Juno waves investigation. *Space Science Reviews*, *213*(1–4), 347–392. https://doi.org/10.1007/s11214-017-0396-y

Lenchek, A., Singer, S., & Wentworth, R. (1961). Geomagnetically trapped electrons from cosmic ray albedo neutrons. *Journal of Geophysical Research*, *66*(12), 4027–4046. https://doi.org/10.1029/jz066i012p04027

Li, W., Ma, Q., Shen, X.-C., Zhang, X.-J., Mauk, B., Clark, G., et al. (2021). Quantification of diffuse auroral electron precipitation driven by whistler mode waves at Jupiter. *Geophysical Research Letters*, *48*(19), e2021GL095457. https://doi.org/10.1029/2021gl095457

Li, W., Ma, Q., Thorne, R., Bortnik, J., Kletzing, C., Kurth, W., et al. (2015). Statistical properties of plasmaspheric hiss derived from Van Allen Probes data and their effects on radiation belt electron dynamics. *Journal of Geophysical Research: Space Physics*, *120*(5), 3393–3405. https://doi.org/10.1002/2015ja021048

Li, W., Thorne, R., Ma, Q., Zhang, X.-J., Gladstone, G., Hue, V., et al. (2017). Understanding the origin of Jupiter's diffuse aurora using Juno's first Perijove observations. *Geophysical Research Letters*, *44*(20), 10–162. https://doi.org/10.1002/2017gl075545

Liu, S., Yan, Q., Yang, C., Zhou, Q., He, Z., He, Y., et al. (2018). Quantifying extremely rapid flux enhancements of radiation belt relativistic electrons associated with radial diffusion. *Geophysical Research Letters*, *45*(3), 1262–1270. https://doi.org/10.1002/2017gl076513

Ma, Q., Li, W., Zhang, X.-J., & Bagenal, F. (2020). Energetic electron scattering due to whistler mode chorus waves using realistic magnetic field and density models in Jupiter's magnetosphere. *Journal of Geophysical Research: Space Physics*, *125*(8), e2020JA027968. https://doi.org/10.1029/2020ja027968

Mauk, B., Williams, D., McEntire, R., Khurana, K., & Roederer, J. (1999). Storm-like dynamics of Jupiter's inner and middle magnetosphere. *Journal of Geophysical Research*, *104*(A10), 22759–22778. https://doi.org/10.1029/1999ja900097

Menietti, J., Averkamp, T., Kurth, W., Faden, J., & Bolton, S. (2023). Survey and analysis of whistler-and Z-mode emission in the Juno extended mission. *Journal of Geophysical Research: Space Physics*, *128*(12), e2023JA032037. https://doi.org/10.1029/2023ja032037

Menietti, J., Averkamp, T., Kurth, W., Imai, M., Faden, J., Hospodarsky, G., et al. (2021). Analysis of whistler-mode and Z-mode emission in the Juno primary mission. *Journal of Geophysical Research: Space Physics*, *126*(11), e2021JA029885. https://doi.org/10.1029/2021ja029885

Menietti, J., Groene, J., Averkamp, T., Horne, R., Woodfield, E., Shprits, Y., et al. (2016). Survey of whistler mode chorus intensity at Jupiter. *Journal of Geophysical Research: Space Physics*, *121*(10), 9758–9770. https://doi.org/10.1002/2016ja022969

Meredith, N. P., Horne, R. B., Sicard-Piet, A., Boscher, D., Yearby, K. H., Li, W., & Thorne, R. M. (2012). Global model of lower band and upper band chorus from multiple satellite observations. *Journal of Geophysical Research*, *117*(A10). https://doi.org/10.1029/2012ja017978

Nénon, Q., Miller, L., Kollmann, P., Liuzzo, L., Pinto, M., & Witasse, O. (2022). Pitch angle distribution of MEV electrons in the magnetosphere of Jupiter. *Journal of Geophysical Research: Space Physics*, *127*(8), e2022JA030627. https://doi.org/10.1029/2022ja030627

Nénon, Q., Sicard, A., & Bourdarie, S. (2017). A new physical model of the electron radiation belts of Jupiter inside Europa's orbit. *Journal of Geophysical Research: Space Physics*, *122*(5), 5148–5167. https://doi.org/10.1002/2017ja023893

Ni, B., Bortnik, J., Nishimura, Y., Thorne, R. M., Li, W., Angelopoulos, V., et al. (2014). Chorus wave scattering responsible for the Earth's dayside diffuse Auroral precipitation: A detailed case study. *Journal of Geophysical Research: Space Physics*, *119*(2), 897–908. https://doi.org/10.1002/2013ja019507

Ni, B., Thorne, R. M., Shprits, Y. Y., & Bortnik, J. (2008). Resonant scattering of plasma sheet electrons by whistler-mode chorus: Contribution to diffuse auroral precipitation. *Geophysical Research Letters*, *35*(11). https://doi.org/10.1029/2008gl034032

Roussos, E., Kollmann, P., Krupp, N., Paranicas, C., Dialynas, K., Sergis, N., et al. (2018). Drift-resonant, relativistic electron acceleration at the outer planets: Insights from the response of Saturn's radiation belts to magnetospheric storms. *Icarus*, *305*, 160–173. https://doi.org/10.1016/j.icarus.2018.01.016

Roussos, E., Krupp, N., Woch, J., Lagg, A., Jones, G., Paranicas, C., et al. (2005). Low energy electron Microsignatures at the orbit of Tethys: Cassini MIMI/LEMMS observations. *Geophysical Research Letters*, *32*(24). https://doi.org/10.1029/2005gl024084

Santos-Costa, D., & Bourdarie, S. (2001). Modeling the inner Jovian electron radiation belt including non-equatorial particles. *Planetary and Space Science*, *49*(3–4), 303–312. https://doi.org/10.1016/s0032-0633(00)00151-3

Schulz, M., & Lanzerotti, L. J. (1974). Particle diffusion in the radiation belts. *Physics and Chemistry in Space*, *7*.

Shprits, Y., Menietti, J., Gu, X., Kim, K.-C., & Horne, R. (2012). Gyroresonant interactions between the radiation belt electrons and whistler mode chorus waves in the radiation environments of Earth, Jupiter, and Saturn: A comparative study. *Journal of Geophysical Research*, *117*(A11). https://doi.org/10.1029/2012ja018031

Shprits, Y., & Ni, B. (2009). Dependence of the quasi-linear scattering rates on the wave normal distribution of chorus waves. *Journal of Geophysical Research*, *114*(A11). https://doi.org/10.1029/2009ja014223

Shprits, Y., Thorne, R., Horne, R., Glauert, S., Cartwright, M., Russell, C., et al. (2006). Acceleration mechanism responsible for the formation of the new radiation belt during the 2003 Halloween solar storm. *Geophysical Research Letters*, *33*(5). https://doi.org/10.1029/2005gl024256

Su, Z., Zheng, H., Chen, L., & Wang, S. (2011). Numerical simulations of storm-time outer radiation belt dynamics by wave–particle interactions including cross diffusion. *Journal of Atmospheric and Solar-Terrestrial Physics*, *73*(1), 95–105. https://doi.org/10.1016/j.jastp.2009.08.002

Subbotin, D., & Shprits, Y. (2009). Three-dimensional modeling of the radiation belts using the Versatile Electron Radiation Belt (VERB) code. *Space Weather*, *7*(10). https://doi.org/10.1029/2008sw000452

Subbotin, D., Shprits, Y., & Ni, B. (2010). Three-dimensional VERB radiation belt simulations including mixed diffusion. *Journal of Geophysical Research*, *115*(A3). https://doi.org/10.1029/2009ja015070

Tao, X., Albert, J. M., & Chan, A. A. (2009). Numerical modeling of multidimensional diffusion in the radiation belts using layer methods. *Journal of Geophysical Research*, *114*(A2). https://doi.org/10.1029/2008ja013826

Tao, X., Bortnik, J., Albert, J. M., & Thorne, R. M. (2012). Comparison of bounce-averaged quasi-linear diffusion coefficients for parallel propagating whistler mode waves with test particle simulations. *Journal of Geophysical Research*, *117*(A10). https://doi.org/10.1029/2012ja017931

Thorne, R., Armstrong, T., Stone, S., Williams, D., McEntire, R., Bolton, S., et al. (1997). Galileo evidence for rapid interchange transport in the Io torus. *Geophysical Research Letters*, *24*(17), 2131–2134. https://doi.org/10.1029/97gl01788

Thorne, R. M., Bortnik, J., Li, W., Chen, L., Ni, B., & Ma, Q. (2016). How whistler-mode waves and thermal plasma density control the global distribution of the diffuse aurora and the dynamical evolution of radiation belt electrons. *Magnetosphere-Ionosphere Coupling in the Solar System*, 115–125. https://doi.org/10.1002/9781119066880.ch9

Tripathi, A., Singhal, R., Singh, K., & Singh, O., II. (2013). Pitch angle diffusion by whistler mode waves in the Jovian magnetosphere and diffuse auroral precipitation. *Icarus*, *225*(1), 424–431. https://doi.org/10.1016/j.icarus.2013.04.016

Van Allen, J. A., Thomsen, M. F., & Randall, B. A. (1980). The energetic charged particle absorption signature of Mimas. *Journal of Geophysical Research*, *85*(A11), 5709–5718. https://doi.org/10.1002/9781118782101.ch6

Wang, D., Shprits, Y. Y., Zhelavskaya, I. S., Agapitov, O. V., Drozdov, A. Y., & Aseev, N. A. (2019). Analytical chorus wave model derived from Van Allen Probe observations. *Journal of Geophysical Research: Space Physics*, *124*(2), 1063–1084. https://doi.org/10.1029/2018ja026183

Woodfield, E., Glauert, S., Menietti, J., Horne, R., Kavanagh, A., & Shprits, Y. (2022). Acceleration of electrons by whistler-mode hiss waves at Saturn. *Geophysical Research Letters*, *49*(3), e2021GL096213. https://doi.org/10.1029/2021gl096213

Woodfield, E., Horne, R., Glauert, S., Menietti, J., & Shprits, Y. (2013). Electron acceleration at Jupiter: Input from cyclotron-resonant interaction with whistler-mode chorus waves. In *Annales Geophysicae* (Vol. 31(10), pp. 1619–1630). https://doi.org/10.5194/angeo-31-1619-2013

Woodfield, E. E., Glauert, S. A., Menietti, J. D., Averkamp, T. F., Horne, R. B., & Shprits, Y. Y. (2019). Rapid electron acceleration in low-density regions of Saturn's radiation belt by whistler mode chorus waves. *Geophysical Research Letters*, *46*(13), 7191–7198. https://doi.org/10.1029/2019gl083071

Woodfield, E. E., Horne, R. B., Glauert, S. A., Menietti, J. D., & Shprits, Y. (2014). The origin of Jupiter's outer radiation belt. *Journal of Geophysical Research: Space Physics*, *119*(5), 3490–3502. https://doi.org/10.1002/2014ja019891

Xiao, F., Su, Z., Zheng, H., & Wang, S. (2010). Three-dimensional simulations of outer radiation belt electron dynamics including cross-diffusion terms. *Journal of Geophysical Research*, *115*(A5). https://doi.org/10.1029/2009ja014541

Xiao, F., Thorne, R., Gurnett, D., & Williams, D. (2003). Whistler-mode excitation and electron scattering during an interchange event near Io. *Geophysical Research Letters*, *30*(14). https://doi.org/10.1029/2003gl017123

Zhao, H., Baker, D., Li, X., Malaspina, D., Jaynes, A., & Kanekal, S. (2019a). On the acceleration mechanism of ultrarelativistic electrons in the center of the outer radiation belt: A statistical study. *Journal of Geophysical Research: Space Physics*, *124*(11), 8590–8599. https://doi.org/10.1029/2019ja027111

Zhao, H., Ni, B., Li, X., Baker, D., Johnston, W., Zhang, W., et al. (2019b). Plasmaspheric hiss waves generate a reversed energy spectrum of radiation belt electrons. *Nature Physics*, *15*(4), 367–372. https://doi.org/10.1038/s41567-018-0391-6